ELSEVIER

Journal of Fluids and Structures 25 (2009) 112–133

JOURNAL OF FLUIDS AND STRUCTURES

www.elsevier.com/locate/jfs

Modelling Pressurized Water Reactor cores in terms of porous media

G. Ricciardi[a,b,*], S. Bellizzi[b], B. Collard[a], B. Cochelin[b]

[a]*CEA CADARACHE DEN/DTN/STRI/LHC, 13108 Saint-Paul-Lez-Durance Cedex, France*
[b]*LMA CNRS, 31 chemin Joseph Aiguier, 13402 Marseille Cedex 20, France*

Received 25 May 2007; accepted 4 April 2008
Available online 3 July 2008

Abstract

The aim of this study is to develop a tractable model of a nuclear reactor core taking the complexity of the structure (including its nonlinear behaviour) and fluid flow coupling into account. The mechanical behaviour modelling includes the dynamics of both the fuel assemblies and the fluid. Each rod bundle is modelled in the form of a deformable porous medium; then, the velocity field of the fluid and the displacement field of the structure are defined over the whole domain. The fluid and the structure are first modelled separately, before being linked together. The equations of motion for the structure are obtained using a Lagrangian approach and, to be able to link up the fluid and the structure, the equations of motion for the fluid are obtained using an arbitrary Lagragian Eulerian approach. The finite element method is applied to spatially discretize the equations. Simulations are performed to analyse the effects of the characteristics of the fluid and of the structure. Finally, the model is validated with a test involving two fuel assemblies, showing good agreement with the experimental data.

Keywords: Fuel assembly; Nonlinear; Porous; Fluid–structure interaction

1. Introduction

The safety of Pressurized Water Reactor (PWR) cores subjected to seismic loading is a major concern in the nuclear industry. A reactor core is a complex structure consisting of 150 fuel assemblies, each of which is composed of 289 regularly spaced rods. Each rod is about 1 cm in diameter, 4 m in length, and the gap between two rods is about 3 mm wide (Fig. 1). There are two types of rod: 25 guide tubes support the other 264 fuel rods that contain enriched uranium. The guide tubes are welded to 10 regularly spaced grids holding fuel rods. The contact points between grids and fuel rods are fitted with springs, so that the fuel rods can slip into the grids. The fuel assemblies are immersed in pressurized water (≈ 15 MPa). The fluid flow is mainly axial, and the transverse component (≈ 0.3 m/s) is small in comparison with the axial component (≈ 5 m/s). Since the fluid velocity is about 5 m/s, the flow is highly turbulent, with a Reynolds number $\mathrm{Re} = 500\,000$ at 300 °C.

*Corresponding author at: CEA CADARACHE DEN/DTN/STRI/LHC, 13108 Saint-Paul-Lez-Durance Cedex, France.
E-mail addresses: guillaume.ricciardi@crans.org (G. Ricciardi), bellizzi@lma.cnrs-mrs.fr (S. Bellizzi), bruno.collard@cea.fr (B. Collard), bruno.cochelin@ec-marseille.fr (B. Cochelin).

0889-9746/$ - see front matter © 2008 Elsevier Ltd. All rights reserved.
doi:10.1016/j.jfluidstructs.2008.04.002

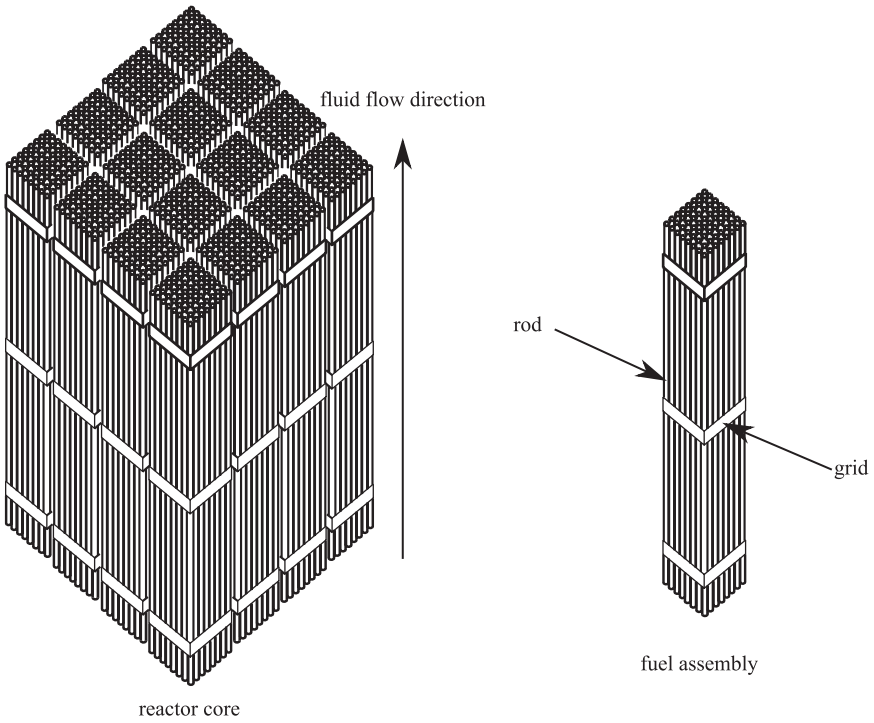

Fig. 1. Part of a reactor core (left); part of a fuel assembly (right).

Modelling a nuclear reactor core involves two main difficulties: the first is the complexity of the structure, which includes nonlinear contact and friction processes (around 30 000 contacts in a fuel assembly). The second one is the presence of the fluid, which gives rise to complex damping, added mass effects, turbulence effects and fuel assembly coupling processes. A direct numerical simulation taking into account the complex geometry, all the nonlinear phenomena, and the fluid–structure interaction would result in too many degrees of freedom. Engineers need simplified models for designing and maintaining reactor cores. Some of these models are briefly reviewed below.

A fuel assembly is frequently modelled in terms of a single beam (Rigaudeau, 1997; Viallet et al., 2003) which is subjected to fluid effects via added mass and damping. These simple models can be used to simulate a row of fuel assemblies and make it possible to perform the large number of simulations required for a statistical seismic loading analysis. Some authors have proposed multi-beam models for simulating a fuel assembly (Ben Jedida, 1993; Fontaine and Politopoulos, 2000) including friction laws to model the rod-grid connections. These models are in good agreement with "in air" experiments, but the friction problems arising are difficult to solve numerically. Broc et al. (2003) proposed a model with two degrees of freedom for each fuel assembly, accounting for the coupling between them, and then developed a linear model for the whole reactor core. Pisapia et al. (2003) and Pisapia (2004) have presented a single-degree-of-freedom nonlinear empirical model for a fuel assembly giving good agreement with "in air" and "in water" experimental data. Most of these models take the fluid effects into account in the form of a linear added mass and an added damping term. Païdoussis (1966, 2003) has used a more complex expression for the fluid forces acting on a fuel assembly, in which the velocity and the relative direction of the flow with respect to the fuel assembly are accounted for. This model, which has been used by Chen (1970), Chen and Wambsganss (1972), Beaud (1997), and Pomîrleanu (2005), gives much better results than the simplified models. However, this complex model does not account for the perturbation of the flow induced by the fuel assemblies' motion. Some authors have proposed to model the fluid flow and the structure using homogenization methods (Jacquelin et al., 1998; Zhang, 1998). In these fluid–structure models, the coupling between fuel assemblies is provided by the fluid flow.

In summary, the main point is that the fluid flow through fuel assemblies induces non-negligible fuel assembly coupling which is not accounted for by most available models. Therefore, we develop a model for the whole reactor core using fluid–structure coupling and porous media theory. This permits to improve the accuracy of the simulation while keeping only a few degrees of freedom. The paper is organized as follows. Section 2 presents the porous media modelling process. Section 3 deals with the fluid forces acting on a rod subjected to a flow. In Section 4, the modelling

equations are developed; the fluid and structure equations are space-averaged to obtain global governing equations, thus each fuel assembly is assimilated to a porous beam, including nonlinear viscoelastic behaviour, and subjected to an axial flow. In Section 5, we briefly present the numerical method. In Section 6 a numerical example modelling two fuel assemblies is proposed. The last section is devoted to the experimental validation of the model on two fuel assemblies subjected to an axial flow.

2. Method

The procedure used to draw up the equations of motion governing the complex fluid/structure entity under investigation is presented in Fig. 2. This procedure is based on a porous medium approach including an equivalent fluid model and an equivalent structure model. Equations of motion for an equivalent fluid and structure are first established separately. For the fluid part, global fluid flow equations through the rod bundle are obtained by spatially averaging the Navier–Stokes equation written with an arbitrary Lagragian Eulerian (ALE) approach. The equivalent fluid, the variables of which are space-averaged, is defined in the whole domain. Structure related effects on the fluid are accounted for by a body force ($\mathbf{F}_{\text{structure}\rightarrow\text{fluid}}$), which is also defined in the whole domain. For the structure part, each fuel assembly is modelled as a porous medium subjected to the body force $\mathbf{F}_{\text{fluid}\rightarrow\text{structure}}$, which is the opposite of the body force $\mathbf{F}_{\text{structure}\rightarrow\text{fluid}}$. Fluid–structure coupling forces are built from fluid forces acting on a rod subjected to an axial flow. Finally, the equivalent structure and equivalent fluid motion equations are both solved with a finite element method.

3. Preliminary: forces acting on a rod

In this section we propose an expression for the fluid force acting on a rod. This expression will be used to model the fluid/structure coupling force in the porous media approach.

3.1. Païdoussis model

For a slender body immersed in a fluid and subjected to a cross-flow, Morison et al. (1950) proposed to decompose the fluid forces into drag and inertial terms. This approach is in good agreement with experiments and has been used in many subsequent studies (Zhou and Graham, 2000; Sarpkaya, 2001). For an axial flow, Païdoussis (1966) proposed an expression for the fluid forces acting on the slender body. His theory based on studies by Lighthill (1960, 1986) and Taylor (1952) has also been widely used (Chen, 1970; Chen and Wambsganss, 1972; Lopes et al., 2002;

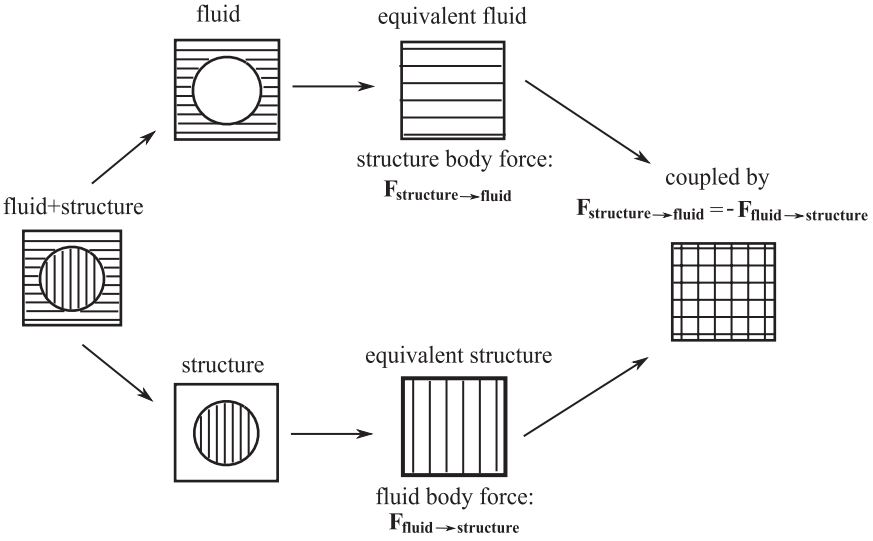

Fig. 2. Porous modelling and method.

Conca et al., 1997). The inviscid term takes the form

$$\mathbf{F}_I = -m_f\left(\frac{\partial}{\partial t} + V_x\frac{\partial}{\partial x}\right)^2 U_y\mathbf{e}_2 - m_f\left(\frac{\partial}{\partial t} + V_x\frac{\partial}{\partial x}\right)^2 U_z\mathbf{e}_3, \tag{1}$$

where U_y is the rod displacement in the $\mathbf{e}_y$ direction, U_z is the rod displacement in the $\mathbf{e}_z$ direction, V_x is the fluid velocity in the $\mathbf{e}_x$ direction, and m_f is a virtual mass per unit length. Viscous forces have transverse components $\mathbf{F}_N$ and $\mathbf{F}_D$, and an axial component $\mathbf{F}_L$:

$$\mathbf{F}_N = -\frac{1}{2}\rho D V_x C_N\left(\frac{\partial U_y}{\partial t} + V_x\frac{\partial U_y}{\partial x}\right)\mathbf{e}_2 - \frac{1}{2}\rho D V_x C_N\left(\frac{\partial U_z}{\partial t} + V_x\frac{\partial U_z}{\partial x}\right)\mathbf{e}_3, \tag{2}$$

$$\mathbf{F}_L = -\tfrac{1}{2}\rho D C_T V_x^2\mathbf{e}_1, \tag{3}$$

$$\mathbf{F}_D = -C\frac{\partial U_y}{\partial t}\mathbf{e}_2 - C\frac{\partial U_z}{\partial t}\mathbf{e}_3, \tag{4}$$

where ρ is the fluid density, D is the rod diameter, and C, C_T and C_N are coefficients which have to be determined; these coefficients depend on the fluid viscosity, the geometry of the structure, and the casing.

3.2. Modified Païdoussis model

The Païdoussis model deals with an axial flow ($V_y = 0$ and $V_z = 0$), but in our model a small transverse component of the flow has to be included ($V_y \neq 0$ and $V_z \neq 0$, Fig. 3). In order to take it into account, we therefore developed a modified Païdoussis model in which the transverse components of the structure velocity are replaced by the transverse structure velocity relative to the fluid flow, for example in the $\mathbf{e}_y$ direction $\partial U_y/\partial t - V_y$.

Expanding first (1) with respect to time and space derivatives gives

$$\begin{aligned}\mathbf{F}_I = &-m_f\left(\frac{\partial}{\partial t}\left(\frac{\partial U_y}{\partial t}\right) + V_x^2\frac{\partial^2 U_y}{\partial x^2} + 2V_x\frac{\partial}{\partial x}\left(\frac{\partial U_y}{\partial t}\right)\right)\mathbf{e}_2\\ &-m_f\left(\frac{\partial}{\partial t}\left(\frac{\partial U_z}{\partial t}\right) + V_x^2\frac{\partial^2 U_z}{\partial x^2} + 2V_x\frac{\partial}{\partial x}\left(\frac{\partial U_z}{\partial t}\right)\right)\mathbf{e}_3,\end{aligned} \tag{5}$$

and replacing the structure velocity by the relative structure–fluid velocity in (2)–(5) gives

$$\begin{aligned}\mathbf{F}_I = &-m_f\left(\frac{\partial}{\partial t}\left(\frac{\partial U_y}{\partial t} - V_y\right) + V_x^2\frac{\partial^2 U_y}{\partial x^2} + 2V_x\frac{\partial}{\partial x}\left(\frac{\partial U_y}{\partial t} - V_y\right)\right)\mathbf{e}_2\\ &-m_f\left(\frac{\partial}{\partial t}\left(\frac{\partial U_z}{\partial t} - V_z\right) + V_x^2\frac{\partial^2 U_z}{\partial x^2} + 2V_x\frac{\partial}{\partial x}\left(\frac{\partial U_z}{\partial t} - V_z\right)\right)\mathbf{e}_3,\end{aligned} \tag{6}$$

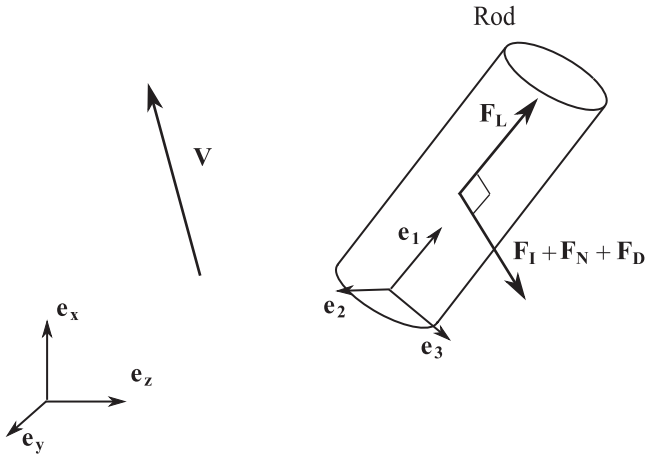

Fig. 3. Rod subjected to axial and transverse flow.

$$\mathbf{F}_N = -\frac{1}{2}\rho D V_x C_N \left(\frac{\partial U_y}{\partial t} - V_y + V_x \frac{\partial U_y}{\partial x}\right)\mathbf{e}_2 - \frac{1}{2}\rho D V_x C_N \left(\frac{\partial U_z}{\partial t} - V_z + V_x \frac{\partial U_z}{\partial x}\right)\mathbf{e}_3, \tag{7}$$

$$\mathbf{F}_L = \tfrac{1}{2}\rho D C_T V_x^2 \mathbf{e}_1, \tag{8}$$

$$\mathbf{F}_D = -C\left(\frac{\partial U_y}{\partial t} - V_y\right)\mathbf{e}_2 - C\left(\frac{\partial U_z}{\partial t} - V_z\right)\mathbf{e}_3, \tag{9}$$

where V_y is the fluid velocity in the $\mathbf{e}_y$ direction, and V_z is the fluid velocity in the $\mathbf{e}_z$ direction. The expressions (6)–(9) will be used in Section 4.3.3 to establish $\mathbf{F}_{\text{fluid}\to\text{structure}}$.

4. Porous model equations

In this section we develop the porous media modelling procedure as described in Section 2. The whole domain of the core including N_{FA} fuel assemblies is noted Ω_c. It is a two-phase parallelepiped containing the fluid and the structure; L_{cx}, L_{cy} and L_{cz} are the dimensions of Ω_c in the $\mathbf{e}_x$, $\mathbf{e}_y$ and $\mathbf{e}_z$ directions. Note that L_{cx} is also the length of a fuel assembly. Ω_c is subdivided into an N_{FA} parallelepiped noted Ω_{FA_i}, each of them containing one fuel assembly.

4.1. Hypotheses

In order to establish equations of motion, we make the following assumptions: the fluid (in this case water) is classically assumed to be viscous, incompressible and Newtonian. Gravity effects are negligible compared to the inertial and viscous forces. As classically assumed in slender body theory, the sections of the rods do not deform, and the presence of grids means that the distance between two rods in a fuel assembly will remain constant. Moreover in order to make easier the writing of the equivalent fluid equations, we assume that the distance between two rods remains constant in the whole core; consequences of that strong hypothesis will be discussed latter in the paper. Turbulent kinetic energy is assumed to be negligible in comparison with the turbulent diffusion.

The hypotheses are recapitulated here:

H1. The fluid is viscous, incompressible and Newtonian.
H2. Gravity effects are neglected.
H3. The rod section does not deform.
H4. Distance between two rods remains constant.
H5. Turbulent kinetic energy is negligible in comparison with the turbulent diffusion.

4.2. Equivalent fluid model

In this section, we establish the equations for an equivalent fluid in Ω_c. We space-average the equations of fluid motion written with an ALE approach. The small-scale turbulence is then modelled with a turbulent viscosity.

4.2.1. ALE approach

Fluid equations are usually written using a Eulerian approach: the fluid is observed through a fixed window. Structure equations are classically written using a Lagrangian approach. In order to be able to relate the fluid and structure equations, we must observe the fluid through the motion of the structure, and we therefore use an ALE approach to write the fluid equations (Duarte et al., 2004). The fluid is observed through a moving window which follows the motion of the structure. It should be noticed that in a general ALE approach, the reference frame can move and deform with an arbitrary velocity.

By using space-averaging methods in the present study, we define an equivalent fluid and an equivalent structure, both of which are defined in the whole domain, so that the displacement of the fluid–structure frontier and the geometric conservation law are included in the space-averaging and the fluid mesh is fixed.

The Navier–Stokes equations written with the ALE approach for an incompressible fluid under assumption H2 give

$$\rho\frac{\partial \mathbf{V}}{\partial t} + \rho\left(\mathbf{V} - \frac{\partial \hat{\mathbf{U}}}{\partial t}\right)\cdot\nabla\mathbf{V} = \operatorname{div}\boldsymbol{\sigma}, \tag{10}$$

$$\operatorname{div}\mathbf{V} = 0, \tag{11}$$

where $\hat{\mathbf{U}}$ is a vector field defined in the whole domain which coincides with the displacement of the structure on the structure domain, $\mathbf{V}$ is the fluid velocity, and $\boldsymbol{\sigma}$ is the Cauchy stress tensor. $\hat{\mathbf{U}}$ will be described more precisely later in the paper. As the fluid is assumed to be Newtonian H1,

$$\boldsymbol{\sigma} = -P\mathbf{I}_d + \mu(\nabla\mathbf{V} + \nabla\mathbf{V}^{\mathrm{T}}), \tag{12}$$

where P is the pressure, μ is the viscosity, and $\mathbf{I}_d$ is the identity tensor.

4.2.2. Space-averaging

Banerjee and Chan (1980) and Delhaye et al. (1981) have established instantaneous space-averaged equations for a two-phase flow, and Robbe and Bliard (2002) have applied this method to a rod bundle. We use the same method as Robbe and Bliard (2002), but we introduce a different structure force.

Let us consider the control volume $\Omega_t(x,y,z)$ centred on the point $M(x,y,z)$ with volume $V_{\Omega_t}(x,y,z) = a \times a \times \mathrm{d}x$ where a is the distance between two rod centres, and $\mathrm{d}x$ is the thickness in the axial direction, with $\mathrm{d}x \ll a$ (Fig. 4(a)):

$$\Omega_t(x,y,z) = \Omega_f(x,y,z) \cup \Omega_s(x,y,z), \tag{13}$$

$$V_{\Omega_t}(x,y,z) = V_{\Omega_f}(x,y,z) + V_{\Omega_s}(x,y,z), \tag{14}$$

where $\Omega_f(x,y,z)$ (respectively, $\Omega_s(x,y,z)$) denotes the fluid (respectively, the structure) domain and $V_{\Omega_f}(x,y,z)$ (respectively, $V_{\Omega_s}(x,y,z)$) is its volume. The frontier of $\Omega_f(x,y,z)$ will be denoted $\partial\Omega_f(x,y,z)$ with

$$\partial\Omega_f(x,y,z) = A_t(x,y,z) \cup A_s(x,y,z), \tag{15}$$

where $A_t(x,y,z)$ is the surface bounding jointly the fluid volume and the control volume, and $A_s(x,y,z)$ is the fluid–structure frontier surface (Fig. 4(b)).

Under assumptions H3 and H4, the fluid fraction present in the control volume does not depend on the control volume position $M(x,y,z)$:

$$V_{\Omega_t}(x,y,z) = V_{\Omega_t}, \quad V_{\Omega_f}(x,y,z) = V_{\Omega_f}, \quad V_{\Omega_s}(x,y,z) = V_{\Omega_s}, \tag{16}$$

and the structure fraction in Ω_t is equal to the volume of a $\mathrm{d}x$ length rod. This will allow us to define the fluid/structure coupling force as force acting on a rod defined in Section 3.

Integrating over the fluid domain $\Omega_f(x,y,z)$, the Navier–Stokes equations (10) and (11) gives

$$\rho \frac{1}{V_{\Omega_t}} \int_{\Omega_f(x,y,z)} \left(\frac{\partial \mathbf{V}}{\partial t} + \left(\mathbf{V} - \frac{\partial \hat{\mathbf{U}}}{\partial t} \right) \cdot \nabla \mathbf{V} \right) \mathrm{d}\Omega = \frac{1}{V_{\Omega_t}} \int_{\Omega_f(x,y,z)} \mathrm{div}\, \boldsymbol{\sigma}\, \mathrm{d}\Omega, \tag{17}$$

$$\frac{1}{V_{\Omega_t}} \int_{\Omega_f(x,y,z)} \mathrm{div}\, \mathbf{V}\, \mathrm{d}\Omega = 0. \tag{18}$$

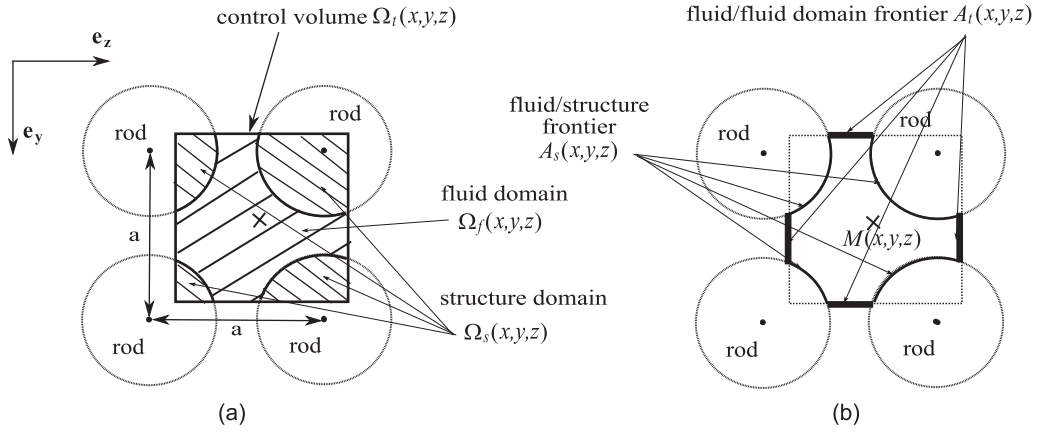

Fig. 4. Control volume for space-averaging.

According to the Leibniz and Gauss theorem, the left-hand-side term of (17) can be transformed as follows:

$$\rho\frac{1}{V_{\Omega_t}}\int_{\Omega_f(x,y,z)}\left(\frac{\partial\mathbf{V}}{\partial t}+\left(\mathbf{V}-\frac{\partial\hat{\mathbf{U}}}{\partial t}\right)\cdot\nabla\mathbf{V}\right)\mathrm{d}\Omega=\rho\frac{1}{V_{\Omega_t}}\frac{\partial}{\partial t}\int_{\Omega_f(x,y,z)}\mathbf{V}\,\mathrm{d}\Omega+\rho\frac{1}{V_{\Omega_t}}\mathrm{div}\int_{\Omega_f(x,y,z)}\mathbf{V}\otimes\mathbf{V}\,\mathrm{d}\Omega$$
$$-\rho\frac{1}{V_{\Omega_t}}\int_{\Omega_f(x,y,z)}\frac{\partial\hat{\mathbf{U}}}{\partial t}\cdot\nabla\mathbf{V}\,\mathrm{d}\Omega-\rho\frac{1}{V_{\Omega_t}}\int_{A_t(x,y,z)}\mathbf{V}\mathbf{n}\cdot\mathbf{V}_{A_t}\,\mathrm{d}S$$
$$-\rho\frac{1}{V_{\Omega_t}}\int_{A_s(x,y,z)}\mathbf{V}\mathbf{n}\cdot\mathbf{V}_{A_s}\,\mathrm{d}S-\rho\frac{1}{V_{\Omega_t}}\int_{A_s(x,y,z)}\mathbf{V}\mathbf{n}\cdot\mathbf{V}\,\mathrm{d}S,\tag{19}$$

where $\mathbf{V}_{A_t}$ is the velocity of the surface $A_t(x,y,z)$, and $\mathbf{V}_{A_s}$ is the velocity of the surface $A_s(x,y,z)$.

Based on the assumptions H3 and H4, the surface integral terms over $A_s(x,y,z)$ cancel. Moreover choosing $\hat{\mathbf{U}}$ constant on the fluid domain Ω_f, the first term of the second line of (19) can be reduced to

$$\rho\frac{1}{V_{\Omega_t}}\int_{\Omega_f(x,y,z)}\frac{\partial\hat{\mathbf{U}}}{\partial t}\cdot\nabla\mathbf{V}\,\mathrm{d}\Omega=\rho\frac{1}{V_{\Omega_t}}\frac{\partial\hat{\mathbf{U}}}{\partial t}\cdot\nabla\int_{\Omega_f(x,y,z)}\mathbf{V}\,\mathrm{d}\Omega,\tag{20}$$

and the second term of the second line of (19) can be transformed after tedious manipulations as

$$\rho\frac{1}{V_{\Omega_t}}\int_{A_t(x,y,z)}\mathbf{V}\mathbf{n}\cdot\mathbf{V}_{A_t}\,\mathrm{d}S=\rho\frac{1}{V_{\Omega_t}}\frac{\partial\hat{\mathbf{U}}}{\partial t}\cdot\nabla\int_{\Omega_f(x,y,z)}\mathbf{V}\,\mathrm{d}\Omega-\rho\frac{1}{V_{\Omega_t}}\int_{\Omega_f(x,y,z)}\mathbf{V}\,\mathrm{d}\Omega\cdot\nabla\frac{\partial\hat{\mathbf{U}}}{\partial t}.\tag{21}$$

Note that $\hat{\mathbf{U}}$ can be chosen constant in the fluid domain because the structure displacement is constant on A_s due to the fact that the structure displacement does not depend on y and z on the structure domain, and that the control volume is thin in the $\mathbf{e}_x$ direction.

Substituting (19)–(21) into (17), and applying the Leibniz and Gauss theorem to the right-hand-side term of (17) and to (18) gives

$$\rho\frac{1}{V_{\Omega_t}}\frac{\partial}{\partial t}\int_{\Omega_f(x,y,z)}\mathbf{V}\,\mathrm{d}\Omega+\rho\frac{1}{V_{\Omega_t}}\mathrm{div}\int_{\Omega_f(x,y,z)}\mathbf{V}\otimes\mathbf{V}\,\mathrm{d}\Omega=2\rho\frac{1}{V_{\Omega_t}}\frac{\partial\hat{\mathbf{U}}}{\partial t}\cdot\nabla\int_{\Omega_f(x,y,z)}\mathbf{V}\,\mathrm{d}\Omega$$
$$-\rho\frac{1}{V_{\Omega_t}}\int_{\Omega_f(x,y,z)}\mathbf{V}\,\mathrm{d}\Omega\cdot\nabla\frac{\partial\hat{\mathbf{U}}}{\partial t}+\frac{1}{V_{\Omega_t}}\mathrm{div}\int_{\Omega_f(x,y,z)}\boldsymbol{\sigma}\,\mathrm{d}\Omega+\frac{1}{V_{\Omega_t}}\int_{A_s(x,y,z)}\boldsymbol{\sigma}\mathbf{n}\,\mathrm{d}S,\tag{22}$$

$$\frac{1}{V_{\Omega_t}}\mathrm{div}\int_{\Omega_f(x,y,z)}\mathbf{V}\,\mathrm{d}\Omega=0.\tag{23}$$

Before establishing governing equations for the averaged velocity $(1/V_{\Omega_f})\int_{\Omega_f(x,y,z)}\mathbf{V}\,\mathrm{d}\Omega$, we have to deal with the convecting term $(\rho/V_{\Omega_t})\mathrm{div}\int_{\Omega_f(x,y,z)}\mathbf{V}\otimes\mathbf{V}\,\mathrm{d}\Omega$ which will be treated by modelling the turbulence.

4.2.3. Turbulence modelling

There are two classical ways of modelling turbulence: by taking the temporal fluctuations that lead to $k-\varepsilon$ models, or by taking the spatial fluctuations that lead to LES models (Barsamian and Hassan, 1997; Hinze, 1975; Lessieur, 1993). Since we use the space-averaging method, the turbulence is modelled here by taking the spatial fluctuations into account.

The fluid velocity can be decomposed into an averaged part and a fluctuating part $\mathbf{V}'$:

$$\mathbf{V}=\frac{1}{V_{\Omega_f}}\int_{\Omega_f(x,y,z)}\mathbf{V}\,\mathrm{d}\Omega+\mathbf{V}',\tag{24}$$

where the averaged value of $\mathbf{V}'$ on $\Omega_f(x,y,z)$ is equal to zero. Substituting (24) into the convective term gives

$$\rho\frac{1}{V_{\Omega_t}}\mathrm{div}\int_{\Omega_f(x,y,z)}\mathbf{V}\otimes\mathbf{V}\,\mathrm{d}\Omega=\rho\frac{1}{V_{\Omega_t}}\mathrm{div}\left(\frac{1}{V_{\Omega_t}}\int_{\Omega_f(x,y,z)}\mathbf{V}\,\mathrm{d}\Omega\otimes\frac{1}{V_{\Omega_t}}\int_{\Omega_f(x,y,z)}\mathbf{V}\,\mathrm{d}\Omega\right)$$
$$+\rho\frac{1}{V_{\Omega_t}}\mathrm{div}\int_{\Omega_f(x,y,z)}\mathbf{V}'\otimes\mathbf{V}'\,\mathrm{d}\Omega,\tag{25}$$

where the last term, which corresponds to turbulence effects in the control volume, refers to the Reynolds tensor $\boldsymbol{\sigma}_{\mathrm{Re}}$:

$$\boldsymbol{\sigma}_{\mathrm{Re}}=\rho\frac{1}{V_{\Omega_t}}\int_{\Omega_f(x,y,z)}\mathbf{V}'\otimes\mathbf{V}'\,\mathrm{d}\Omega.\tag{26}$$

Classically, the Reynolds tensor is modelled by the turbulent viscosity model proposed by Smagorinsky (1963):

$$\boldsymbol{\sigma}_{\mathrm{Re}} = -\frac{2}{3}\rho k_T I_d + \mu_T \left(\nabla \frac{1}{V_{\Omega_t}} \int_{\Omega_f(x,y,z)} \mathbf{V}\, \mathrm{d}\Omega + \left(\nabla \frac{1}{V_{\Omega_t}} \int_{\Omega_f(x,y,z)} \mathbf{V}\, \mathrm{d}\Omega \right)^{\mathrm{T}} \right), \tag{27}$$

where μ_T is the turbulent viscosity, and k_T is the turbulent kinetic energy (which is equal to the kinetic energy of the fluctuating velocity). Under assumption H5, $\frac{2}{3}\rho k_T I_d$ can be neglected and, as the flow in a PWR is mostly homogeneous, μ_T is chosen constant in time and space.

4.2.4. Equivalent fluid

Let us define the equivalent fluid, the variables of which are

$$\mathbf{V}_{\mathrm{eq}} = \frac{1}{V_{\Omega_f}} \int_{\Omega_f(x,y,z)} \mathbf{V}\, \mathrm{d}\Omega, \tag{28}$$

$$P_{\mathrm{eq}} = \beta \frac{1}{V_{\Omega_f}} \int_{\Omega_f(x,y,z)} P\, \mathrm{d}\Omega. \tag{29}$$

Substituting (28) and (29) into (22) and (23), and using (27) gives

$$\rho_{\mathrm{eq}} \frac{\partial \mathbf{V}_{\mathrm{eq}}}{\partial t} + \rho_{\mathrm{eq}} \mathrm{div}\, \mathbf{V}_{\mathrm{eq}} \otimes \mathbf{V}_{\mathrm{eq}} = -\nabla P_{\mathrm{eq}} + \mu_{T\mathrm{eq}} \Delta \mathbf{V}_{\mathrm{eq}} + 2\rho_{\mathrm{eq}} \frac{\partial \hat{\mathbf{U}}}{\partial t} \cdot \nabla \mathbf{V}_{\mathrm{eq}} - \rho_{\mathrm{eq}} \mathbf{V}_{\mathrm{eq}} \cdot \nabla \frac{\partial \hat{\mathbf{U}}}{\partial t} + \mathbf{F}_{\mathrm{structure}\to\mathrm{fluid}}, \tag{30}$$

$$\mathrm{div}\, \mathbf{V}_{\mathrm{eq}} = 0, \tag{31}$$

where $\rho_{\mathrm{eq}} = \beta\rho$, $\mu_{T\mathrm{eq}} = \beta(\mu_T + \mu)$, with $\beta = V_{\Omega_f}/V_{\Omega_t}$ denotes the porosity, and

$$\mathbf{F}_{\mathrm{structure}\to\mathrm{fluid}} = \frac{1}{V_{\Omega_t}} \int_{A_s(x,y,z)} \boldsymbol{\sigma}\mathbf{n}\, \mathrm{d}S. \tag{32}$$

We recognize in the first line of (30) the classical equation of an incompressible Newtonian fluid of density ρ_{eq}, and viscosity $\mu_{T\mathrm{eq}}$ written with an ALE approach. This equation contains two additional terms. The first $\rho_{\mathrm{eq}}\mathbf{V}_{\mathrm{eq}} \cdot \nabla \partial \hat{\mathbf{U}}/\partial t$ results from the space-averaging of the ALE formulation. The second term $\mathbf{F}_{\mathrm{structure}\to\mathrm{fluid}}$ represents the structure body force acting on the fluid (Fig. 2). Finally, the equivalent fluid can be considered as a single substance filling the whole domain Ω_c. It is governed by (30) and (31).

4.3. Equivalent structure model

In this section, we establish the equations for an equivalent structure in Ω_{FA_i} to model a fuel assembly. We space-average the structure motion equations as classically done with porous media. Since the fuel assembly is a slender body, we use Timoshenko beam assumptions to transform the 3-D equilibrium equations into beam reduced equations. The constitutive laws for the beam are obtained from semi-empirical considerations.

4.3.1. Space-averaging

As in the fluid case, we space-average the equation of motion of the structure over the structure domain $\Omega_s(x,y,z)$ (Fig. 4):

$$\rho_s \frac{1}{V_{\Omega_t}} \int_{\Omega_s(x,y,z)} \frac{\partial^2 \mathbf{U}}{\partial t^2}\, \mathrm{d}\Omega = \frac{1}{V_{\Omega_t}} \int_{\Omega_s(x,y,z)} \mathrm{div}\, \boldsymbol{\sigma_s}\, \mathrm{d}\Omega, \tag{33}$$

where $\mathbf{U}$ is the structure displacement, ρ_s is the structure density, and $\boldsymbol{\sigma_s}$ is the Cauchy stress tensor.

According to the Leibniz and Gauss theorem, and under assumptions H3 and H4, Eq. (33) becomes

$$(1-\beta)\rho_s \frac{\partial^2}{\partial t^2} \left(\frac{1}{V_{\Omega_s}} \int_{\Omega_s(x,y,z)} \mathbf{U}\, \mathrm{d}\Omega \right) = (1-\beta)\mathrm{div} \left(\frac{1}{V_{\Omega_s}} \int_{\Omega_s(x,y,z)} \boldsymbol{\sigma_s}\, \mathrm{d}\Omega \right) + \frac{1}{V_{\Omega_t}} \int_{A_s(x,y,z)} \boldsymbol{\sigma_s}\mathbf{n}\, \mathrm{d}S. \tag{34}$$

As previously done with the fluid, let us define an equivalent structure with variables

$$\mathbf{U}_{\mathrm{eq}} = \frac{1}{V_{\Omega_s}} \int_{\Omega_s(x,y,z)} \mathbf{U}\, \mathrm{d}\Omega, \tag{35}$$

$$\boldsymbol{\sigma}_{\text{seq}} = \frac{1}{V_{\Omega_s}} \int_{\Omega_s(x,y,z)} \boldsymbol{\sigma}_s \, \mathrm{d}\Omega. \tag{36}$$

Eq. (34) can be rewritten as

$$\rho_{\text{seq}} \frac{\partial^2 \mathbf{U}_{\text{eq}}}{\partial t^2} = (1-\beta)\mathrm{div}\, \boldsymbol{\sigma}_{\text{seq}} + \mathbf{F}_{\text{fluid}\to\text{structure}}, \tag{37}$$

where $\rho_{\text{seq}} = (1-\beta)\rho_s$ and

$$\mathbf{F}_{\text{fluid}\to\text{structure}} = \frac{1}{V_{\Omega_t}} \int_{A_s(x,y,z)} \boldsymbol{\sigma}_s \mathbf{n} \, \mathrm{d}S. \tag{38}$$

We recognize in (37), the classical Newton's law for a continuous structure written on the deformed configuration with the density ρ_{seq} and a body force $\mathbf{F}_{\text{fluid}\to\text{structure}}$ which represents the fluid body force acting on the structure (Fig. 2). The transport of (37) to the fixed undeformed configuration gives [see Holzapfel (2000)]:

$$\rho_{\text{seq}} \frac{\partial^2 \mathbf{U}_{\text{eq}}}{\partial t^2} = (1-\beta)\mathrm{div}\,((\mathbf{I}_d + \nabla \mathbf{U}_{\text{eq}})\mathbf{S}_{\text{seq}}) + J\mathbf{F}_{\text{fluid}\to\text{structure}}, \tag{39}$$

where $\mathbf{S}_{\text{seq}}$ is the second Piola–Kirchhoff stress tensor, and J is the volume ratio between the reference and the current configuration. Under assumptions H3 and H4, the motion is volume-preserving ($J = 1$ and does not depend on time and position); therefore the body force expression is the same in the reference and the current configuration. Finally, an equivalent structure, for each fuel assembly, can be considered as a single substance filling the domain Ω_{FA_i} (Fig. 5(a)). Note that since each fuel assembly has its own displacement, the displacement field defined on the whole domain Ω_c is continuous in part: the discontinuities are located on the frontiers delimiting fuel assembly domains $\partial\Omega_{FA_i}$.

4.3.2. Kinematics of a fuel assembly

Because of the dimensions of a fuel assembly, we can use a beam hypothesis to model the equivalent structure. Since it was observed that the shear stiffness of a fuel assembly is very low, the Euler–Bernoulli approximation is not satisfied, and we shall therefore use a Timoshenko beam model. The kinematics of a Timoshenko beam are defined by the displacement of the mean line $\mathbf{u}_{\text{eq}}$ and the rotation of the cross-section $\boldsymbol{\theta}_{\text{eq}}$ (Fig. 5(b)).

The displacement $\mathbf{U}_{\text{eq}}(x,y,z)$ of a fuel assembly point which is not located on the mean line is given by

$$\mathbf{U}_{\text{eq}}(x,y,z) = \mathbf{u}_{\text{eq}}(x) + \boldsymbol{\theta}_{\text{eq}}(x) \wedge (y\mathbf{e}_y + z\mathbf{e}_z). \tag{40}$$

4.3.3. Fluid–structure coupling force

In order to couple fluid and structure, the equivalent fluid model is written with $\hat{\mathbf{U}} = \mathbf{U}_{\text{eq}}$, and the fluid–structure coupling force $\mathbf{F}_{\text{structure}\to\text{fluid}}$ is specified as a function of $\mathbf{U}_{\text{eq}}$ and $\mathbf{V}_{\text{eq}}$. Darcy and Forcheimer have proposed some simple expressions for $\mathbf{F}_{\text{structure}\to\text{fluid}}$ [see Costa et al. (2004), Fourar et al. (2004) and Zhang et al. (2003)] assuming the inertial effects negligible and the porosity isotropic, which is suitable for porous media modelling in soil and oil research purposes. Since these assumptions are not valid dealing with our problem, we propose a model based on the modified Païdoussis expression presented in Section 3.

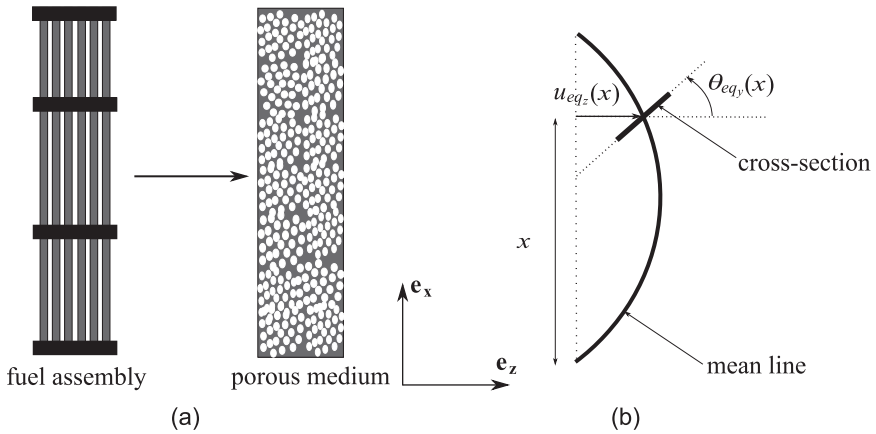

Fig. 5. (a) Porous medium model; (b) kinematics of a Timoshenko beam.

Recalling that the control volume contains one rod, the structure/fluid body force brought to $M(x,y,z)$ is defined from (6)–(9) as (Fig. 6)

$$\mathbf{F}_{\text{structure}\to\text{fluid}} = -\frac{1}{S}(\mathbf{F}_I + \mathbf{F}_N + \mathbf{F}_D + \mathbf{F}_L), \tag{41}$$

where $S = a^2$.

Substituting (40) into (41), projecting it on the base $(\mathbf{e}_x,\mathbf{e}_y,\mathbf{e}_z)$ and neglecting second order terms gives

$$\begin{aligned}
\mathbf{F}_{\text{structure}\to\text{fluid}} = {} & \frac{m_f}{S}\left(\frac{\partial}{\partial t}\left(\frac{\partial u_{\text{eq}_y}}{\partial t} - V_{\text{eq}_y}\right) + V_{\text{eq}_x}^2\frac{\partial^2 u_{\text{eq}_y}}{\partial x^2} + 2V_{\text{eq}_x}\frac{\partial}{\partial x}\left(\frac{\partial u_{\text{eq}_y}}{\partial t} - V_{\text{eq}_y}\right)\right)\mathbf{e}_y \\
& + \frac{1}{S}\left(\frac{1}{2}\rho D V_{\text{eq}_x} C_N\left(\frac{\partial u_{\text{eq}_y}}{\partial t} - V_{\text{eq}_y} + V_{\text{eq}_x}\frac{\partial u_{\text{eq}_y}}{\partial x}\right) + C\left(\frac{\partial u_{\text{eq}_y}}{\partial t} - V_{\text{eq}_y}\right)\right)\mathbf{e}_y \\
& + \frac{m_f}{S}\left(\frac{\partial}{\partial t}\left(\frac{\partial u_{\text{eq}_z}}{\partial t} - V_{\text{eq}_z}\right) + V_{\text{eq}_x}^2\frac{\partial^2 u_{\text{eq}_z}}{\partial x^2} + 2V_{\text{eq}_x}\frac{\partial}{\partial x}\left(\frac{\partial u_{\text{eq}_z}}{\partial t} - V_{\text{eq}_z}\right)\right)\mathbf{e}_z \\
& + \frac{1}{S}\left(\frac{1}{2}\rho D V_{\text{eq}_x} C_N\left(\frac{\partial u_{\text{eq}_z}}{\partial t} - V_{\text{eq}_z} + V_{\text{eq}_x}\frac{\partial u_{\text{eq}_z}}{\partial x}\right) + C\left(\frac{\partial u_{\text{eq}_z}}{\partial t} - V_{\text{eq}_z}\right)\right)\mathbf{e}_z \\
& - \frac{1}{2S}\rho D C_T V_{\text{eq}_x}^2\mathbf{e}_x - \frac{1}{2S}\rho D C_T V_{\text{eq}_x}^2\frac{\partial u_{\text{eq}_y}}{\partial x}\mathbf{e}_y - \frac{1}{2S}\rho D C_T V_{\text{eq}_x}^2\frac{\partial u_{\text{eq}_z}}{\partial x}\mathbf{e}_z.
\end{aligned} \tag{42}$$

The model is completely defined, given the numerical values of the coefficients m_f, C, C_T and C_N which depend on the geometry, the roughness and the casing.

The fluid force acting on a fuel assembly is given by the integration over the fuel assembly cross-section of the fluid body force $\mathbf{F}_{\text{fluid}\to\text{structure}}$:

$$\mathbf{F}_{\text{fluid}\to FA} = \int_{S_{fa}} \mathbf{F}_{\text{fluid}\to\text{structure}}\,\mathrm{d}S, \tag{43}$$

$$\mathbf{M}_{\text{fluid}\to FA} = \int_{S_{fa}} (y\mathbf{e}_y + z\mathbf{e}_z) \wedge \mathbf{F}_{\text{fluid}\to\text{structure}}\,\mathrm{d}S, \tag{44}$$

where S_{fa} is the area of the cross-section of a fuel assembly.

4.3.4. Dynamic equations

Since the transverse displacement of the fuel assembly remains small as compared to the size of its cross-section the geometrical nonlinearities are limited to the moderate rotations assumption. The 3-D dynamic equations (39) are reduced to following beam form (Chia, 1980):

$$m_{fa}\frac{\partial^2 u_{\text{eq}_x}}{\partial t^2} = \frac{\partial T}{\partial x} + \mathbf{F}_{\text{fluid}\to FA}\cdot\mathbf{e}_x, \tag{45}$$

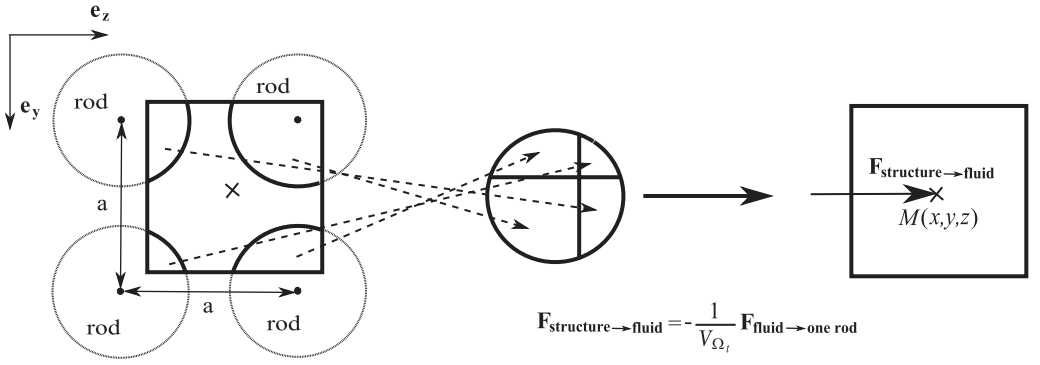

Fig. 6. Modelling of structure/fluid coupling body force.

$$m_{fa}\frac{\partial^2 u_{\mathrm{eq}_y}}{\partial t^2}=\frac{\partial Q_y}{\partial x}+\frac{\partial}{\partial x}\left(T\frac{\partial u_{\mathrm{eq}_y}}{\partial x}\right)+\mathbf{F}_{\mathrm{fluid}\to FA}\cdot\mathbf{e}_y, \tag{46}$$

$$m_{fa}\frac{\partial^2 u_{\mathrm{eq}_z}}{\partial t^2}=\frac{\partial Q_z}{\partial x}+\frac{\partial}{\partial x}\left(T\frac{\partial u_{\mathrm{eq}_z}}{\partial x}\right)+\mathbf{F}_{\mathrm{fluid}\to FA}\cdot\mathbf{e}_z, \tag{47}$$

$$I_{fa}\frac{\partial^2 \boldsymbol{\theta}_{\mathrm{eq}}}{\partial t^2}=\frac{\partial \mathbf{M}}{\partial x}+\mathbf{e}_1\wedge\mathbf{Q}+\mathbf{M}_{\mathrm{fluid}\to FA}, \tag{48}$$

where m_{fa} is the mass per unit length of a fuel assembly, I_{fa} is the inertial moment per unit length of a fuel assembly, T is the tension force, $\mathbf{M}=M_y\mathbf{e}_y+M_z\mathbf{e}_z$ is the bending moment and $\mathbf{Q}=Q_y\mathbf{e}_y+Q_z\mathbf{e}_z$ is the shear force.

In the following we make explicit the term T. Neglecting $\partial^2 u_{\mathrm{eq}_x}/\partial t^2$ in (45) gives

$$\frac{\partial T}{\partial x}+\frac{1}{S}\int_{S_{fa}}F_{L_x}\,\mathrm{d}S=0, \tag{49}$$

where F_{L_x} denotes the component of $\mathbf{F}_L$ on the $\mathbf{e}_x$ direction. Assuming that $\mathbf{F}_L$ is constant along the $\mathbf{e}_x$ direction and integrating (49) gives

$$T=T_0-x\frac{1}{S}\int_{S_{fa}}F_{L_x}\,\mathrm{d}S, \tag{50}$$

where T_0 is the tension force at the bottom of the fuel assembly, and has to be identified as a parameter.

Substituting (50) and (43) in (46) and (47) gives

$$m_{fa}\frac{\partial^2 u_{\mathrm{eq}_y}}{\partial t^2}=\frac{\partial Q_y}{\partial x}+T_0\frac{\partial^2 u_{\mathrm{eq}_y}}{\partial x^2}+\frac{1}{S}\int_{S_{fa}}\left(F_{I_y}+F_{N_y}+F_{D_y}-xF_{L_x}\frac{\partial^2 u_{\mathrm{eq}_y}}{\partial x^2}\right)\mathrm{d}S, \tag{51}$$

$$m_{fa}\frac{\partial^2 u_{\mathrm{eq}_z}}{\partial t^2}=\frac{\partial Q_z}{\partial x}+T_0\frac{\partial^2 u_{\mathrm{eq}_z}}{\partial x^2}+\frac{1}{S}\int_{S_{fa}}\left(F_{I_z}+F_{N_z}+F_{D_z}-xF_{L_x}\frac{\partial^2 u_{\mathrm{eq}_z}}{\partial x^2}\right)\mathrm{d}S, \tag{52}$$

where the subscript y (respectively, subscript z) refers to the component on the $\mathbf{e}_y$ (respectively, $\mathbf{e}_z$) direction.

4.3.5. Constitutive laws of the beam

The coupling between grids and rods gives rise to complex contact and friction processes which make it difficult to establish the analytical overall constitutive laws from the bending law of the rods and the friction law. It is therefore proposed to model the global nonlinear behaviour of the fuel assembly empirically. Pisapia et al. (2003) and Pisapia (2004) have observed that the results obtained using models based on the quadratic stiffness and quadratic damping give good agreement with the experimental data. Here a quadratic law is used for the stiffness, whereas the damping is assumed to be linear. In fact the structural damping is very small in comparison with the fluid damping, so it is useless to refine it. The bending moment $\mathbf{M}$ and the shear force $\mathbf{Q}$ are related to kinematic unknowns by

$$Q_y=G_1S_{fa}\left(\frac{\partial u_{\mathrm{eq}_y}}{\partial x}-\theta_{\mathrm{eq}_z}\right)+G_2S_{fa}\left|\frac{\partial u_{\mathrm{eq}_y}}{\partial x}-\theta_{\mathrm{eq}_z}\right|\left(\frac{\partial u_{\mathrm{eq}_y}}{\partial x}-\theta_{\mathrm{eq}_z}\right)+\mu_GS_{fa}\frac{\partial}{\partial t}\left(\frac{\partial u_{\mathrm{eq}_y}}{\partial x}-\theta_{\mathrm{eq}_z}\right), \tag{53}$$

$$Q_z=G_1S_{fa}\left(\frac{\partial u_{\mathrm{eq}_z}}{\partial x}+\theta_{\mathrm{eq}_y}\right)+G_2S_{fa}\left|\frac{\partial u_{\mathrm{eq}_z}}{\partial x}+\theta_{\mathrm{eq}_y}\right|\left(\frac{\partial u_{\mathrm{eq}_z}}{\partial x}+\theta_{\mathrm{eq}_y}\right)+\mu_GS_{fa}\frac{\partial}{\partial t}\left(\frac{\partial u_{\mathrm{eq}_z}}{\partial x}+\theta_{\mathrm{eq}_y}\right), \tag{54}$$

$$M_y=E_1I\frac{\partial\theta_{\mathrm{eq}_y}}{\partial x}+E_2I\left|\frac{\partial\theta_{\mathrm{eq}_y}}{\partial x}\right|\left(\frac{\partial\theta_{\mathrm{eq}_y}}{\partial x}\right)+\mu_EI\frac{\partial^2\theta_{\mathrm{eq}_y}}{\partial t\partial x}, \tag{55}$$

$$M_z=E_1I\frac{\partial\theta_{\mathrm{eq}_z}}{\partial x}+E_2I\left|\frac{\partial\theta_{\mathrm{eq}_z}}{\partial x}\right|\left(\frac{\partial\theta_{\mathrm{eq}_z}}{\partial x}\right)+\mu_EI\frac{\partial^2\theta_{\mathrm{eq}_z}}{\partial t\partial x}, \tag{56}$$

where G_1, G_2, E_1, E_2 are stiffness coefficients, μ_G, μ_E are structural damping coefficients, and I is the quadratic moment of inertia.

4.4. Coupled model

We have built an equivalent fluid model (30) and (31) defined in Ω_c, using the vector field $\hat{\mathbf{U}}$, and an equivalent structure model (37) defined for each fuel assembly in Ω_{FA_i}. Thus, for each particle of Ω_c, a structure variable coexists with a fluid variable.

We can now summarize the equivalent model for the fluid–structure problem: we have to solve the coupled equations in Ω_c,

$$\rho_{\text{eq}}\frac{\partial \mathbf{V}_{\text{eq}}}{\partial t}+\rho_{\text{eq}}\text{div}\,\mathbf{V}_{\text{eq}}\otimes\mathbf{V}_{\text{eq}}=-\nabla P_{\text{eq}}+\mu_{T\text{eq}}\Delta\mathbf{V}_{\text{eq}}+2\rho_{\text{eq}}\frac{\partial \mathbf{u}_{\text{eq}}}{\partial t}\cdot\nabla\mathbf{V}_{\text{eq}}-\rho_{\text{eq}}\mathbf{V}_{\text{eq}}\cdot\nabla\frac{\partial \mathbf{u}_{\text{eq}}}{\partial t}+\mathbf{F}_{\text{structure}\to\text{fluid}}, \tag{57}$$

$$\text{div}\,\mathbf{V}_{\text{eq}}=0, \tag{58}$$

$$m_{fa}\frac{\partial^2 u_{\text{eq}_y}}{\partial t^2}=\frac{\partial Q_y}{\partial x}+T_0\frac{\partial^2 u_{\text{eq}_y}}{\partial x^2}+\frac{1}{S}\int_{S_{fa}}\left(F_{I_y}+F_{N_y}+F_{D_y}-xF_{L_x}\frac{\partial^2 u_{\text{eq}_y}}{\partial x^2}\right)\text{d}S, \tag{59}$$

$$m_{fa}\frac{\partial^2 u_{\text{eq}_z}}{\partial t^2}=\frac{\partial Q_z}{\partial x}+T_0\frac{\partial^2 u_{\text{eq}_z}}{\partial x^2}+\frac{1}{S}\int_{S_{fa}}\left(F_{I_z}+F_{N_z}+F_{D_z}-xF_{L_x}\frac{\partial^2 u_{\text{eq}_z}}{\partial x^2}\right)\text{d}S, \tag{60}$$

$$I_{fa}\frac{\partial^2 \boldsymbol{\theta}_{\text{eq}}}{\partial t^2}=\frac{\partial \mathbf{M}}{\partial x}+\mathbf{e}_1\wedge\mathbf{Q}+\mathbf{M}_{\text{fluid}\to FA}, \tag{61}$$

with

$$\mathbf{u}_{\text{eq}}=\sum_{i=1}^{N_{FA}}\mathbf{u}_{\text{eq}_i}\mathbb{I}_{\Omega_{FA_i}},\quad \boldsymbol{\theta}_{\text{eq}}=\sum_{i=1}^{N_{FA}}\boldsymbol{\theta}_{\text{eq}_i}\mathbb{I}_{\Omega_{FA_i}}, \tag{62}$$

where $\mathbf{V}_{\text{eq}}$, P_{eq}, $\mathbf{u}_{\text{eq}_i}$ and $\boldsymbol{\theta}_{\text{eq}_i}$ are the unknowns, and $\mathbb{I}_{\Omega_{FA_i}}$ denotes the indicator function of Ω_{FA_i}.

The unknowns have to satisfy some boundary conditions as follows for each instant noted t.

(i) Fuel assemblies are clamped at their ends, which means displacements and rotations are set equal to zero:

$$\mathbf{u}_{\text{eq}_i}(0,t)=0,\quad \mathbf{u}_{\text{eq}_i}(L_{cx},t)=0;\quad \boldsymbol{\theta}_{\text{eq}_i}(0,t)=0,\quad \boldsymbol{\theta}_{\text{eq}_i}(L_{cx},t)=0. \tag{63,64}$$

(ii) The fluid velocity is imposed on the inlet and the outlet, and supposed to be homogeneous:

$$\forall(y,z),\ \mathbf{V}_{\text{eq}}(L_{cx},y,z,t)=V_{bc}\mathbf{e}_x,\quad \mathbf{V}_{\text{eq}}(0,y,z,t)=V_{bc}\mathbf{e}_x, \tag{65}$$

where V_{bc} is the constant value of the imposed velocity.

(iii) At the walls a non-penetration condition of the fluid is imposed:

$$\forall(x,z),\ \mathbf{V}_{\text{eq}}(x,0,z,t)\cdot\mathbf{e}_y=0,\quad \mathbf{V}_{\text{eq}}(x,L_{cy},z,t)\cdot\mathbf{e}_y=0, \tag{66}$$

$$\forall(x,y),\ \mathbf{V}_{\text{eq}}(x,y,0,t)\cdot\mathbf{e}_z=0,\quad \mathbf{V}_{\text{eq}}(x,y,L_{cz},t)\cdot\mathbf{e}_z=0. \tag{67}$$

4.5. Discussion

We have built a global model of the behaviour of a PWR to avoid the large number of degrees of freedom necessary to make a direct numerical simulation of the fluid and structure dynamics. We have transformed a fluid–structure problem with a complex geometry (large number of rods linked by numerous contact friction points) into a problem with a more simple geometry (equivalent beam for each fuel assembly). It becomes possible to simulate both the fluid and the structure dynamics of a whole core. Some local information is lost compared to a direct numerical simulation, such as vibrations of rods into grids, but interactions between fuel assemblies, via fluid or contacts, are conserved. For example the effects of an external excitation (such as an earthquake or plane crash) on the impact forces between fuel assemblies can be simulated.

The physical problem includes several scales (Fig. 7) which have been taken into account: the reactor core is made up of fuel assemblies, fuel assemblies are made up of rods which correspond to the control volume scale, and the small-scale turbulence are accounted for by a turbulent viscosity model.

The proposed model needs several coefficients: some of them are given by the geometry and physical characteristics of materials involved in the problem (m_{fa}, I_{fa}, S_{fa}, I, ρ, ρ_{eq}, $\mu_{T\text{eq}}$, L_{cx}, D and S), the others are introduced by empirical modelling and have to be identified by experiments (G_1, G_2, E_1, E_2, μ_G, μ_E, m_f, C_N, C_T and C). T_0 results from a compressive spring it therefore induces a decrease of the stiffness.

Unknowns of both equivalent fluid and structure are defined in the whole domain Ω_c, which means that, in the proposed model, there is no pure fluid zone accounted for. We assumed that distance between two rods remains constant H4, but this is no more true (in the physical problem) at the interfaces between fuel assemblies, so pure fluid

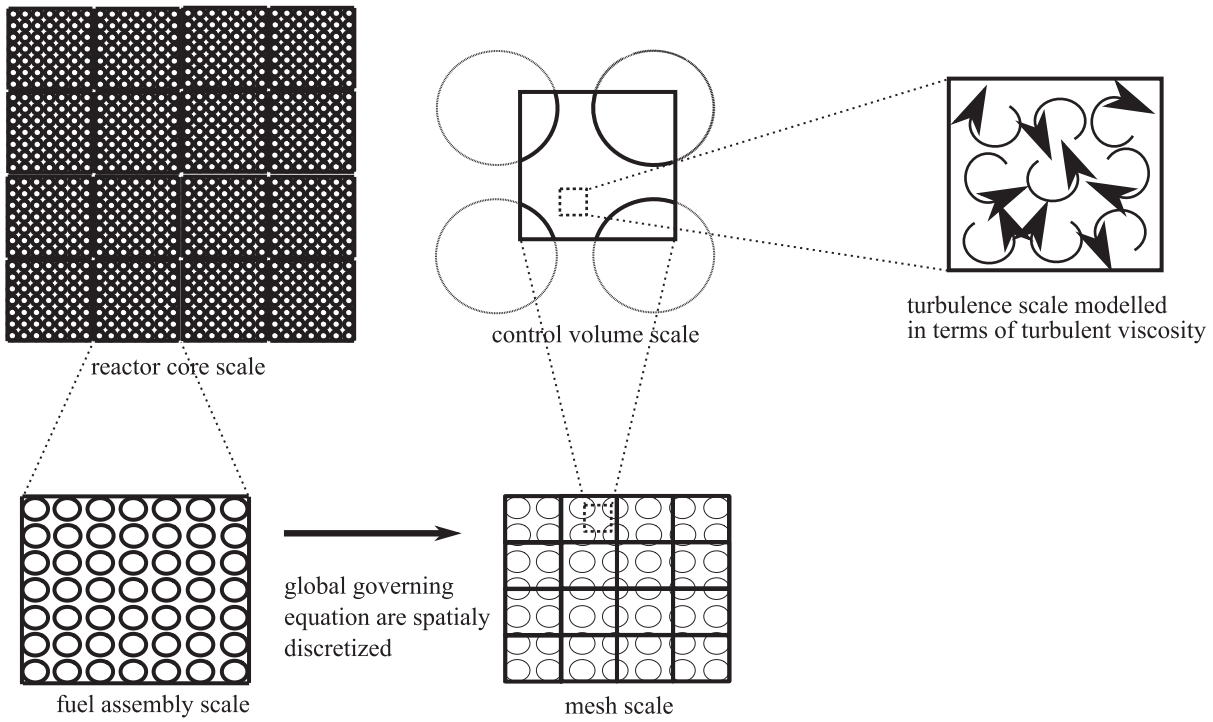

Fig. 7. The scales of the problem.

zones appear at those interfaces and between fuel assemblies and walls. The size of the pure fluid zones changes in time as the fuel assemblies move, and it could induce additional fluid forces on the fuel assemblies at the interfaces.

5. Numerical model

The variational formulation of Eqs. (57)–(61) is spatially discretized using the finite element method. In the case of the 2-D model, we use a $Q9/4$ mixed "velocity–pressure" element, the velocity of the fluid is discretized with nine nodes, and the continuous pressure with four nodes. In addition, the structure field (Timoshenko beams) is discretized using a 3-node beam element. In the case of the 3-D model, we use a $Q27/8$ mixed "velocity–pressure" element, the velocity of the fluid is discretized with 27 nodes, and the continuous pressure with eight nodes. The structure field is discretized using a 3-node beam element in each direction. The spatial mesh of a single fuel assembly is shown in Fig. 8. For the fluid, the finite element mesh covers the whole domain of the fuel assembly. For the structure, the mesh is 1-D. Based on the kinematics (40), the degrees of freedom are the displacements and the rotations of the nodes on the mean line of the beam. Therefore, one structure element (for instance $S1$ in Fig. 8) is superimposed on several fluid elements (for instance $F1$, $F2$, $F3$, $F4$ and $F5$ in Fig. 8). Thus the number of degrees of freedom related to the fluid is larger than those related to the structure. Note that it is necessary to ensure that the mesh scale is smaller than the fuel assembly scale in order to obtain significant results, but it must be larger than the control volume scale, otherwise the physical relevance of the space-averaging procedure would be lost (Fig. 7).

For the temporal discretization procedure, two different classical schemes were chosen to discretize the fluid and structure equations, the fluid equations (57) and (58) are temporally discretized with an Uzawa scheme [see Langtangen et al. (2002)], and the structure equations (59)–(61) are discretized with a Newmark scheme [see Krenk (2006)]. At each time step, the following nonlinear system has to be solved:

$$\begin{pmatrix} A_F(\mathbf{v}_{k+1},\mathbf{u}_{k+1}) & \alpha\Delta t B & H_F(\mathbf{v}_{k+1}) \\ B^{\mathrm{T}} & 0 & 0 \\ H_S(\mathbf{v}_{k+1}) & 0 & A_S(\mathbf{v}_{k+1},\mathbf{u}_{k+1}) \end{pmatrix} \begin{pmatrix} \mathbf{v}_{k+1} \\ \mathbf{p}_{k+1} \\ \mathbf{u}_{k+1} \end{pmatrix} = \begin{pmatrix} G_k \\ 0 \\ L_k \end{pmatrix}, \tag{68}$$

where $\mathbf{v}_{k+1}$ is the fluid velocity vector discretized unknown, $\mathbf{p}_{k+1}$ is the fluid pressure vector discrete unknown, $\mathbf{u}_{k+1}$ is the structure vector discrete unknown, and k refers to the kth time step. Spatial and temporal discretizations give the linear

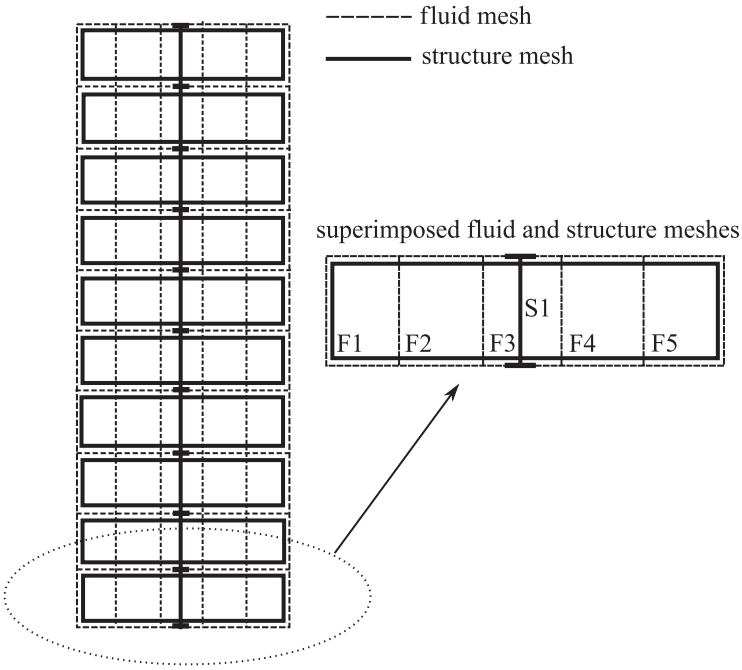

Fig. 8. Fluid and structure mesh used to discretize one fuel assembly.

and nonlinear matrix: $A_F(\mathbf{v}_{k+1}, \mathbf{u}_{k+1})$, B, $H_F(\mathbf{v}_{k+1})$, $H_S(\mathbf{v}_{k+1})$, $A_S(\mathbf{v}_{k+1}, \mathbf{u}_{k+1})$, G_k, and L_k. The nonlinear system is solved with Newton's method.

6. Numerical example

In this section, free oscillations of two fuel assemblies subjected to a flow (see Fig. 9) are simulated, first in 2-D and second in 3-D.

6.1. 2-D simulations

Dynamic 2-D simulations of two fuel assemblies subjected to a 3 m/s axial flow were performed using coefficients given in Tables 1–4, and with the following discretization parameters: six fluid and structure elements in the axial direction and eight fluid elements in the transverse direction (four fluid elements for each fuel assembly), and a time step $\Delta t = 0.013$ s. Fig. 10 shows the displacements of the third grids from the bottom of the left and right fuel assemblies versus time; the initial shape deformation of the left fuel assembly (with an amplitude of 10 mm) was imposed, whereas the right one was initially at rest. At $t = 0$ the system is set free of external forces; we observe that while the left fuel assembly returns to its equilibrium position, the right fuel assembly starts to oscillate before finally returning to its equilibrium position. That is the result of the coupling between fuel assemblies and water: the left fuel assembly induces a perturbation in the fluid flow. As a result, the fluid applies forces on the right fuel assembly and makes it oscillate.

Fig. 11 shows the displacement of the third grid of the left fuel assembly versus time obtained with three temporal discretizations (right) and 13 spatial discretizations (from 6 to 12 elements in the axial and transverse directions) (left). The convergence study shows that the numerical model is stable considering the time discretization (Fig. 11, left). Convergence of the spatial parameters is gradually achieved, and six elements in the axial direction, and eight elements in the transverse direction give accurate enough results.

6.2. 3-D simulations

Dynamic 3-D simulations of two fuel assemblies subjected to a 3 m/s axial flow were performed with six fluid and structure elements in the $\mathbf{e}_x$ direction, eight fluid elements in the $\mathbf{e}_z$ direction (four fluid elements for each fuel assembly),

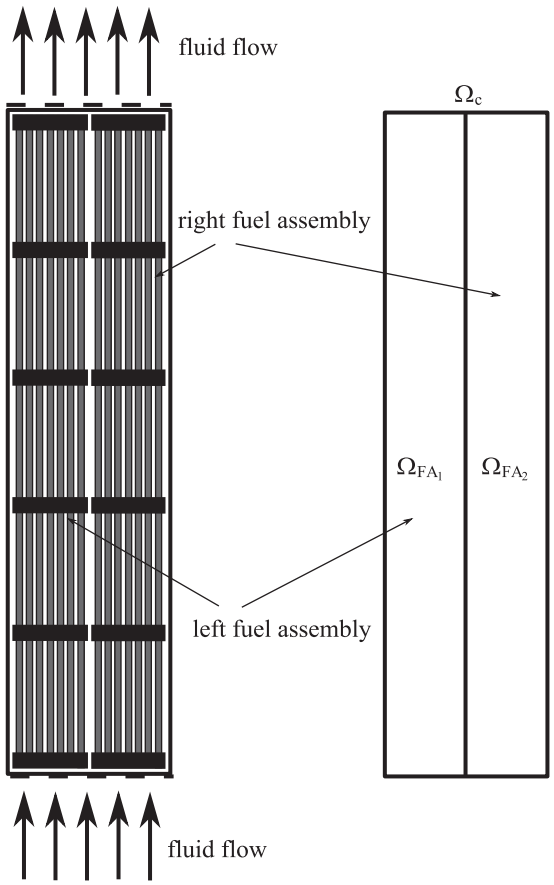

Fig. 9. Modelling of two fuel assemblies subjected to an axial flow.

Table 1
Geometrical and inertial coefficients related to the structure; Eqs. (59)–(61)

m_{fa}	I_{fa}	S_{fa}	I	L_{cx}
60 kg/m	0.59 kg m	1.19×10^{-2} m^2	1.19×10^{-5} m^4	2.75 m

Table 2
Coefficients related to the structure behaviour; Eqs. (59)–(61)

G_1	G_2	E_1	E_2	μ_G	μ_E
2×10^7 Pa	-2×10^7 Pa	5×10^8 Pa	-6×10^8 Pa	6×10^4 Pa s	4×10^6 Pa s

Table 3
Fluid coefficients; Eq. (57)

ρ	ρ_{eq}	μ_{Teq}
1000 kg/m^3	532.44 kg/m^3	0.1 kg m^2/s

Table 4
Coefficients related to fluid/structure coupling; Eq. (42)

m_f	C_T	C_N	C	D	S
$0.3\,\mathrm{kg/m^3}$	$0.3\,\mathrm{m^{-2}}$	$3\,\mathrm{m^{-2}}$	$30\,\mathrm{kg/s}$	$0.01\,\mathrm{m}$	$1\times10^{-4}\,\mathrm{m^2}$

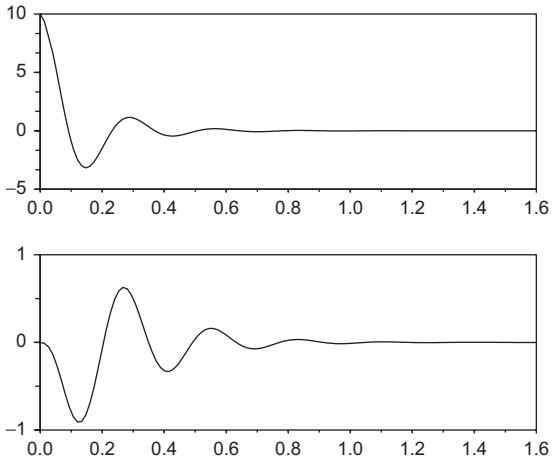

Fig. 10. Displacement (mm) versus time (s) of the third grid of the left fuel assembly (top), and of the right fuel assembly (bottom) resulting from the numerical simulation with coefficients of Tables 1–4, in 3 m/s water flow.

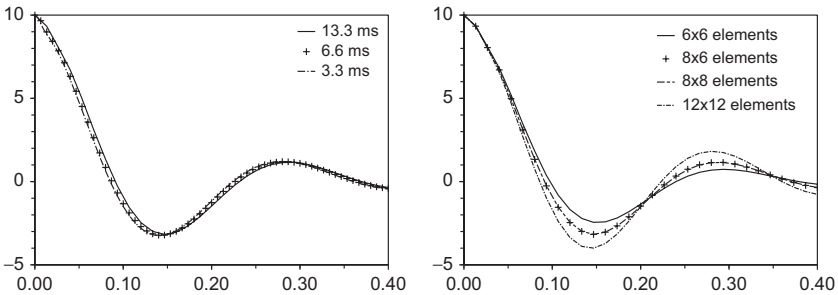

Fig. 11. Displacement (mm) versus time (s) of the third grid of the left fuel assembly for different time discretizations (left), and different spatial discretizations (right).

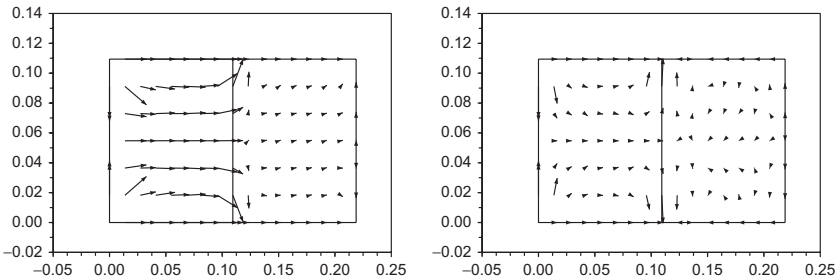

Fig. 12. Fluid velocity field 3-D numerical estimation in the middle horizontal cross-section at $t = 0.09$ s (left), and at $t = 0.15$ s (right).

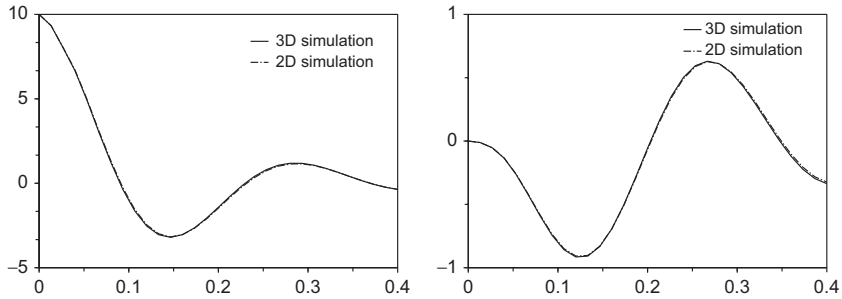

Fig. 13. Displacement (mm) versus time (s) of the third grid of the left fuel assembly (left), and of the right fuel assembly (right): comparison of 2-D/3-D simulations.

three fluid elements in the $\mathbf{e}_y$ direction and a time step $\Delta t = 0.013$ s, an initial displacement of the left the fuel assembly is imposed in the $\mathbf{e}_z$ direction. The 3-D simulations show that convergence in the $\mathbf{e}_y$ direction was achieved with one element. Fig. 12 shows the transverse fluid velocity field (V_{eq_y} and V_{eq_z}) on the horizontal cross-section located at the level of the third grid; at 0.09 s the two fuel assemblies move in the same direction, whereas at 0.15 s they move in opposite directions. The fluid flow is mostly in the $\mathbf{e}_z$ direction, except at the interface between the fuel assemblies. The 2-D and 3-D comparisons show similar fuel assembly displacements (Fig. 13). However, 3-D simulations involve much more degrees of freedom (and CPU time) than 2-D simulations and do not provide more precise results for the chosen configuration.

7. Experimental validation

In this section, we compare the experimental data and numerical results obtained for two fuel assemblies subjected to an axial flow.

7.1. Experimental apparatus

Fig. 14 shows the experimental apparatus used to test the validity of the model. The experimental apparatus includes two reduced scale fuel assemblies (8×8 rods for a length of 2.75 m) subjected to an axial flow. The gap between fuel assemblies and between fuel assemblies and the casing is about 1 mm, except for the casing on the left of the left fuel assembly: the experimental apparatus includes a 10 mm wide bypass on the left of the left fuel assembly, which is necessary to be able to trigger the initial displacement. This experimental device was initially designed to study impacts between fuel assemblies [see Collard and Vallory (2001)]. An initial displacement is imposed on the third grid of the left fuel assembly, and the right fuel assembly is in its equilibrium state. At $t = 0$ the system is set free of external forces, and free oscillations are therefore observed. Tests were performed in air and in water at various fluid velocities from 0 to 5.2 m/s which is close to reactor operating conditions, and with various initial displacements from 1 to 10 mm. Displacements of the third grids are measured with a laser Doppler velocimetry technique.

7.2. Coefficient identification

Both the 2-D and 3-D numerical models are used in simulations to be described. The model includes several coefficients that have to be chosen. A first set of coefficients was calculated analytically (m_{fa}, I_{fa}, S_{fa}, I, ρ, ρ_{eq}, $\mu_{T\mathrm{eq}}$, L_{cx}, D and S). A second set including only structural coefficients (G_1, G_2, E_1, E_2, μ_G, μ_E) was identified from the in air experiments. The identification process was based on the minimization of the cost function:

$$F_{\mathrm{cost}}(G_1, G_2, E_1, E_2, \mu_G, \mu_E) = \sum_{i=1}^{N_{\mathrm{sample}}} \frac{|d_{\mathrm{exp}}(ti) - d_{\mathrm{sim}}(ti, G_1, G_2, E_1, E_2, \mu_G, \mu_E)|}{|d_{\mathrm{exp}}(ti)|}, \tag{69}$$

where d_{sim} is the simulated displacement and d_{exp} is the experimental one. As structural coefficients are identified from in-air experiments, T_0 is accounted for in the stiffness coefficients, thus we have to choose $T_0 = 0$. We can see in Fig. 15 the displacement of a fuel assembly in air obtained by the experiment and by the simulation after optimization for a 1 cm initial displacement. We can notice that the period of oscillations decreases in time (first period 0.26 s, second

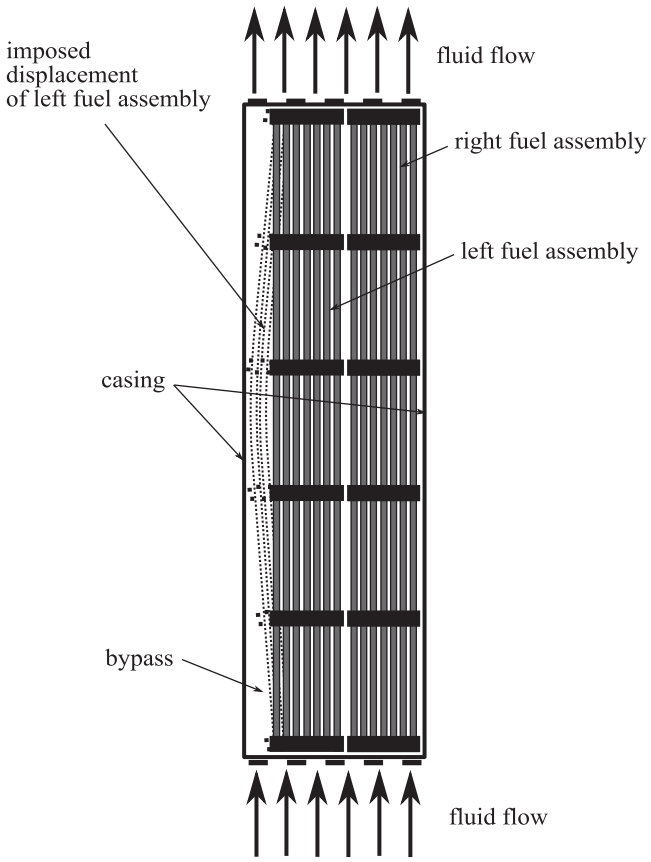

Fig. 14. Experimental apparatus.

period 0.245 s and third period 0.24 s), which means that the stiffness decreases with displacement, so nonlinear structure effects have to be accounted for. The set of coefficients obtained by an optimization on the in-air experimental data with an initial displacement of 1 cm was kept for simulating the other initial displacements. It was also kept for performing the in-water simulations.

The last set of coefficients including only the coupling coefficients (m_f, C_N, C_T and C) was first determined by performing pressure measurements through rod bundles subjected to fluid flow, and then empirically adjusted on 5.2 m/s experimental displacements. Those coefficients depend on the geometry of the structure, its roughness, the material, and the casing (for coupling coefficients), but they do not depend on fluid flow conditions and the type of excitation. For reasons of confidentiality, the coefficients used in the following simulations are not delivered in this paper.

7.3. Results

Fig. 16 shows the initial conditions of the fuel assemblies and fluid flow, obtained by resolving the statics problem. We can see that the right fuel assembly is deformed by the flow induced by the deformation of the left fuel assembly. This process is well-observed experimentally.

Simulations were performed with two initial conditions. In the first case described above (Fig. 16), the initial conditions have been chosen equal to the statics problem. In the second case, the fluid flow is assumed to be homogeneous, and the displacement of the right fuel assembly is set to zero. Results show that the initial conditions do not greatly affect the fuel assembly displacements, thus the simulations that follow are performed with the second initial condition.

Fig. 17 presents the simulation for two different fluid velocities: 2.4 and 5.2 m/s. The results of the simulations are in good agreement with the experimental data on the left assembly: the damping increases with the axial fluid velocity, and

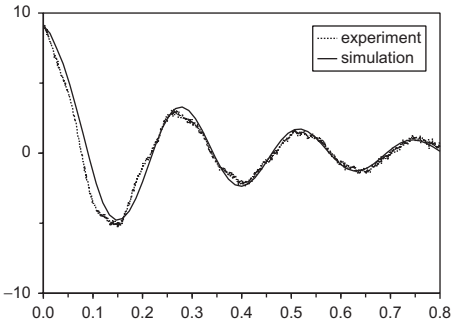

Fig. 15. Displacement (mm) versus time (s) of the third grid of the left fuel assembly in air: comparison of numerical simulations/experimental data (dashed line).

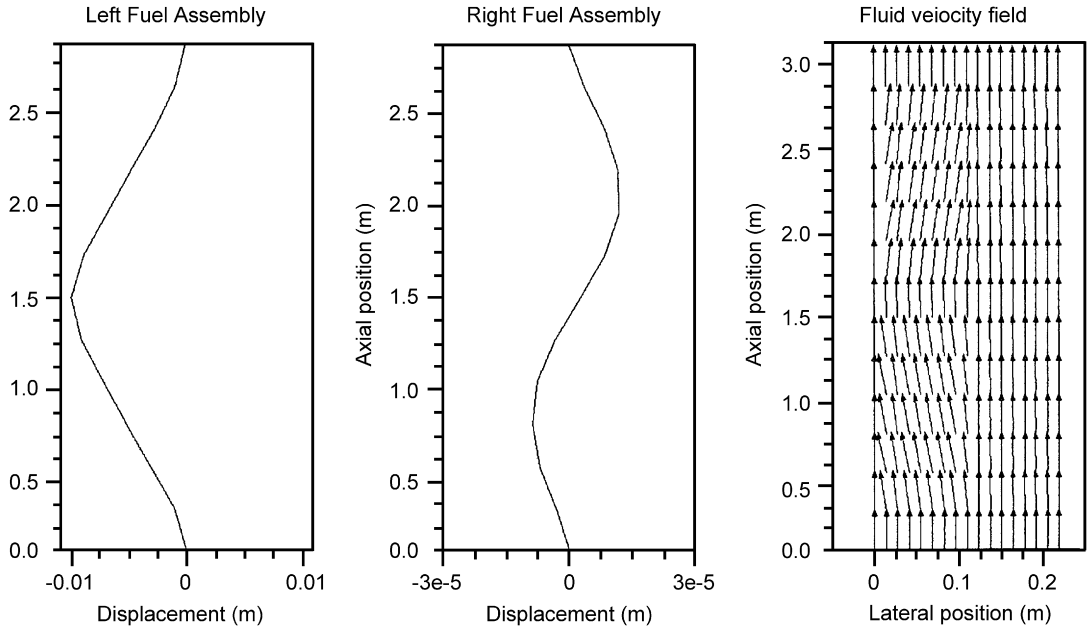

Fig. 16. 2-D numerical simulation of static response (initial configuration).

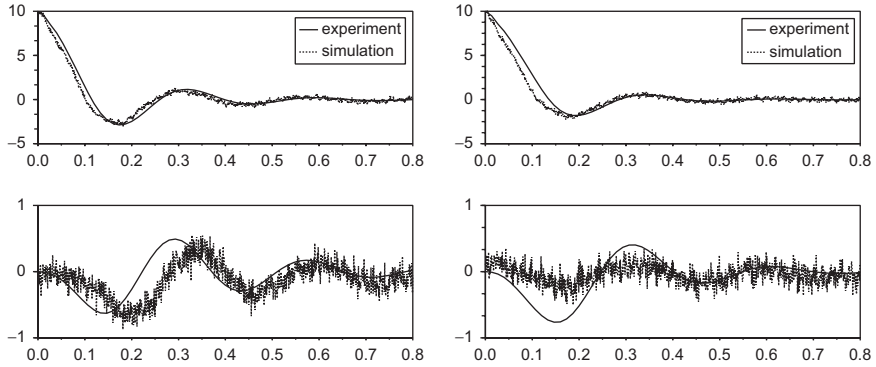

Fig. 17. Displacement (mm) versus time (s) of the third grid of the left fuel assembly (top) and of the right fuel assembly (bottom) for 2.4 m/s water flow (left), and 5.2 m/s water flow (right): comparison of simulations/experimental data.

the coupling between fuel assemblies via the fluid is reproduced. However, the energy transmitted to the right fuel assembly seems to be overestimated at high fluid velocities. The presence of the bypass in the experimental device induces an asymmetric fluid flow, and the fluid velocity is higher in the left fuel assembly than in the right one: the fluid velocity profile depends on the fluid velocity because of the nonlinear effects, and the bypass is not taken into account in the numerical model (Fig. 9), which explains why the coupling is overestimated.

The numerical simulation of the right fuel assembly is out of phase with the experimental curve, possibly due to the variations of the gap between the fuel assemblies, which induces changes in the porosity, which is assumed to be constant in the model (see Section 4.5).

We can see in Fig. 17 that a 10 mm initial displacement of the left fuel assembly induces a non-negligible 1 mm displacement of the right fuel assembly. This illustrates the importance of the influence of the fluid dynamics on the structure dynamics, and justifies the modelling of a coupled fluid–structure system.

We have seen that the model reasonably reproduces the fuel assembly dynamics, but it seems to be useless as we have to perform experiments to obtain the coefficients used in the model. However, the aim of the model is not to simulate two fuel assemblies but a row of fuel assemblies and finally a whole core. So, coefficients can be obtained with low cost experiments on a few fuel assemblies with appropriate casing, and used afterward to simulate more fuel assemblies under various operating conditions. For instance, various configurations mixing end-of-life and beginning-of-life fuel assemblies can be analysed under various excitation conditions, such as seismic loading.

The coefficients were identified on high level experimental data (initial displacement of 1 cm, and fluid velocity of 5.2 m/s), and simulations of lower fluid velocities and initial displacements showed good agreement with experiments.

8. Instability

Païdoussis (1966) established numerically that a rod subjected to axial flow becomes unstable when the fluid velocity reaches a critical value. As the model presented here is based on Païdoussis's theory, instability is observed at very high fluid velocities. The model predicts instability at fluid velocities greater than 33.9 m/s. In reactor operating conditions the velocity is about 5 m/s which is nearly 10 times lower than the critical value obtained by simulations. Accordingly, there is no risk that instability occurs in practice.

Fig. 18 shows 2-D simulations of the displacement of the fuel assembly middle node, when the fuel assembly is subjected to very high velocity flow. The fuel assembly vibrates at a frequency of 8.3 Hz, which is around three times higher than the natural frequency observed with lower velocities flows. Fig. 19 shows the shape deformation of the fuel assembly for those high fluid velocities; the fluid inlet is located at the bottom of the figure.

The instability is due to the fluid term $-\rho DC_N/(2S)V_{\mathrm{eq}_x}^2\partial u_{\mathrm{eq}_y}/\partial x$ in Eq. (42) which becomes dominant with high velocities as it increases with the square of the fluid velocity $V_{\mathrm{eq}_x}^2$, whereas the damping is proportional to V_{eq_x}. The fluid force at the bottom is in the opposite direction to that at the head top of the fuel assembly as $\partial u_{\mathrm{eq}_y}/\partial x$ changes of sign, and it therefore induces coupling between structural modes: the first mode excites the second one and so on, and this causes the fuel assembly to vibrate in a high frequency mode.

The displacement occurring far from the fluid inlet is greater than that occurring near it (Fig. 19). This difference in amplitude is due to the term $-\rho DC_T/(2S)xV_{\mathrm{eq}_x}^2\partial^2 u_{\mathrm{eq}_y}/\partial x^2$ in (42) which increases with x and is maximal at the top of the fuel assembly.

9. Conclusion

In this study, an overall model for a nuclear reactor core has been developed using a porous medium method. One of the main features of this model is the account of the dynamics of both the fluid and the structure, the nonlinear behaviour of the fuel assemblies, and the fluid–structure coupling. Fuel assemblies are assimilated to porous media with nonlinear viscoelastic behaviour. The fluid equations are written in the ALE framework, and space-averaged in order to determine the overall behaviour of the fluid. The fluid–structure coupling is provided by a body force based on fluid forces acting on a rod subjected to an axial flow. Numerical 2-D and 3-D models were drawn up using a finite element method for the spatial discretization. The temporal discretization is performed using two classical schemes, for the structure, and for the fluid. The results of the numerical simulations are in good agreement with the experimental data. The effect of the fluid velocity on the damping of the structure is well reproduced, whereas the coupling between fuel assemblies is qualitatively reproduced.

Because of the averaged character of porous media equations, we have transformed a fluid–structure problem with a complex geometry (large number of rods linked by numerous contact friction points) into a problem with a more simple

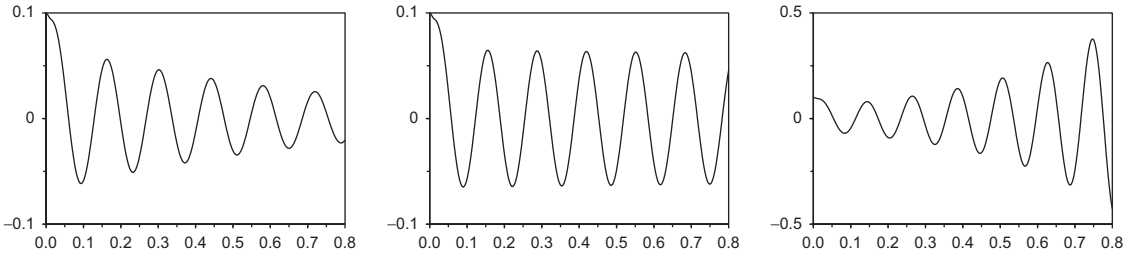

Fig. 18. Fuel assembly displacement (mm) versus time (s) in the case of 33 m/s water flow (left) (stable regime), a 33.9 m/s water flow (middle) (critical regime), and a 35.5 m/s water flow (right) (unstable regime).

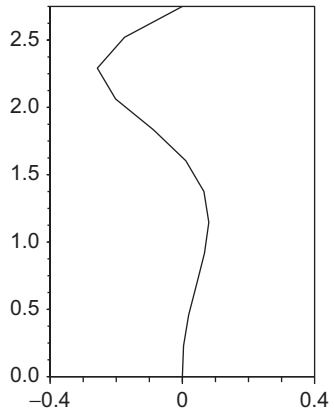

Fig. 19. Fuel assembly shape deformation at high velocity flow rates, axial position (m) versus displacement (mm).

geometry (equivalent beam for each fuel assembly). That permitted to model a fuel assembly with few degrees of freedom, thus a large number of fuel assemblies can be simulated.

Further studies including sinusoidal and seismic excitations with a larger number of fuel assemblies are in progress. Experiments on a 3×3 fuel assembly network subjected to an axial flow will be performed and the results compared with numerical simulations.

References

Banerjee, S., Chan, A.M.C., 1980. Analysis of the averaged and local instantaneous formulations. International Journal of Multiphase Flow 6, 1–24.

Barsamian, H.R., Hassan, Y.A., 1997. Large eddy simulation of turbulent crossflow in tube bundles. Nuclear Engineering and Design 172, 103–122.

Beaud, F., 1997. An analytical model for the prediction of fluidelastic forces in a rod bundle subjected to axial flow: theory, experimental validation and application to PWR fuel assemblies. In: 5th International Conference on Nuclear Engineering, Nice, France, ICONE5-2290. Elsevier, Amsterdam.

Ben Jedida, A., 1993. Etude du comportement sismique d'un coeur de réacteur nucléaire de type REP. Thèse de doctorat, Université Paris VI.

Broc, D., Queval, J.C., Viallet, E., 2003. Seismic behaviour of a PWR reactor core: fluid structure interaction effects. In: Vejvoda, S. (Ed.), Transactions of the 17th International Conference on Structural Mechanics in Reactor Technology (SMIRT 17), Prague, Czech Republic, Paper K14-2.

Chen, S.S., 1970. Free vibration of a coupled fluid/structural system. Journal of Sound and Vibration 21, 387–398.

Chen, S.S., Wambsganss, M.W., 1972. Parallel-flow induced vibrations of fuel rods. Nuclear Engineering and Design 18, 253–278.

Chia, C.Y., 1980. Non-linear Analysis of Plates. McGraw-Hill, New York.

Collard, B., Vallory, J., 2001. Impact forces on a core shroud of an exited PWR fuel assembly. In: 9th International Conference on Nuclear Engineering, Nice Acropolis, France, ICONE9-1783. Elsevier, Amsterdam.

Conca, C., Osses, A., Planchard, J., 1997. Added mass and damping in fluid–structure interaction. Computer Methods in Applied Mechanics and Engineering 146, 387–405.
Costa, V.A.F., Oliveira, M.S.A., Sousa, A.C.M., 2004. Numerical simulation of non-Darcian flows through spaces partially filled with a porous medium. Computers and Structures 82, 1535–1541.
Delhaye, J.M., Giot, M., Riethmuller, M.L., 1981. Thermohydraulics of two-phase systems for industrial design and nuclear engineering. In: A von Karman Institute Book. Hemisphere Publishing Corporation, McGraw-Hill, New York.
Duarte, F., Gormaz, R., Natesan, S., 2004. Arbitrary Lagrangian–Eulerian method for Navier–Stokes equations with moving boundaries. Computer Methods in Applied Mechanics and Engineering 193, 4819–4836.
Fontaine, B., Politopoulos, I., 2000. A non-linear model for the PWR fuel assembly seismic analysis. Nuclear Engineering and Design 195, 321–329.
Fourar, M., Radilla, G., Lenormand, R., Moyne, C., 2004. On the non-linear behavior of a laminar single-phase flow through two and three-dimensional porous media. Advances in Water Resources 27, 669–677.
Hinze, J.O., 1975. Turbulence. McGraw-Hill, New York.
Holzapfel, G.A., 2000. Nonlinear Solid Mechanics. A Continuum Approach for Engineering. Wiley, Chichester.
Jacquelin, E., Lainé, J.P., Trollat, C., Jézéquel, L., 1998. Modelling the behaviour of a PWR core by a homogenization technique. Computer Methods in Applied Mechanics and Engineering 155, 1–13.
Krenk, S., 2006. Energy conservation in Newmark based time integration algorithms. Computer Methods in Applied Mechanics and Engineering 195, 6110–6124.
Langtangen, H.P., Mardal, K.A., Winther, R., 2002. Numerical methods for incompressible viscous flow. Advances in Water Resources 25, 1125–1146.
Lessieur, M., 1993. Turbulence in Fluids. Kluwer Academic Publishers, Dordrecht.
Lighthill, M.J., 1960. Note on the swimming and slender fish. Journal of Fluid Mechanics 9, 305–317.
Lighthill, M.J., 1986. Fundamentals concerning wave loading on offshore structures. Journal of Fluid Mechanics 173, 667–681.
Lopes, J.L., Païdoussis, M.P., Semler, C., 2002. Linear and nonlinear dynamics of cantilevered cylinders in axial flow. Part 2: the equations of motion. Journal of Fluid and Structures 16, 715–737.
Morison, J.R., O'Brien, M.P., Johnson, J.W., Schaaf, S.A., 1950. The forces exerted by surface waves on piles. Petroleum Transactions, AIME 189, 149–157.
Païdoussis, M.P., 1966. Dynamics of flexible slender cylinders in axial flow. Part 1: theory. Journal of Fluid Mechanics 26, 717–736.
Païdoussis, M.P., 2003. Fluid–Structure Interactions: Slender Structures and Axial Flow, vol. 2. Elsevier Academic Press, London.
Pisapia, S., 2004. Etude du comportement vibratoire non-linéaire d'un assemblage combustible de réacteur à eau pressurisée. Thèse de doctorat de l'Université de la Méditerranée Aix-Marseille.
Pisapia, S., Collard, B., Bellizzi, S., Mori, V., 2003. Modal testing and identification of a PWR fuel assembly. In: Vejvoda, S. (Ed.), Transactions of the 17th International Conference on Structural Mechanics in Reactor Technology (SMIRT 17), Prague, Czech Republic, Paper C01-4.
Pomîrleanu, R.O., 2005. Spectral response to harmonic excitation of rods in a confined nuclear fuel mini-bundle. In: Proceedings of PVP 2005: ASME Pressure Vessels and Piping Division conference, Denver Colorado Paper 71486. ASME, New York.
Rigaudeau, J., 1997. Grid modelling and strength criterion in the lateral response of PWR fuel assemblies under accident conditions. In: 5th International Conference on Nuclear Engineering, Nice, France, ICONE5-2568. Elsevier, Amsterdam.
Robbe, M.F., Bliard, F., 2002. A porosity method to describe the influence of internal structures on a fluid flow in case of fast dynamics problems. Nuclear Engineering and Design 215, 217–242.
Sarpkaya, T., 2001. On the force decompositions of Lighthill and Morison. Journal of Fluids and Structures 15, 227–233.
Smagorinsky, J., 1963. General circulation experiments with primitive equations. Monthly Weather Review 91, 216–241.
Taylor, G.I., 1952. Analysis of the swimming of long and narrow animals. Proceedings of the Royal Society London A 214, 158–184.
Viallet, E., Bolsee, G., Ladouceur, B., Goubin, T., Rigaudeau, J., 2003. Validation of PWR core seismic models with shaking table tests on interacting scale 1 fuel assemblies. In: Vejvoda, S. (Ed.), Transactions of the 17th International Conference on Structural Mechanics in Reactor Technology (SMIRT 17), Prague, Czech Republic, Paper C01-2.
Zhang, R.J., 1998. Structural homogenized analysis for a nuclear reactor core. Nuclear Engineering and Design 183, 151–156.
Zhang, H., Zhang, X., Ji, S., Guo, Y., Ledezma, G., Elabbasi, N., deCougny, H., 2003. Recent development of fluid–structure interaction capabilities in the ADINA system. Computers and Structures 81, 1071–1085.
Zhou, C.Y., Graham, J.M.R., 2000. A numerical study of cylinders in waves and currents. Journal of Fluids and Structures 14, 403–428.